COLUMN RESTRAINING EFFECTS IN POST-TENSIONED SELF-CENTERING MOMENT FRAMES

C.C. Chou[1] and J.H. Chen[2]

[1] *Associate Professor, Dept. of Civil Engineering, Taiwan University, Taipei, Chinese Taiwan*
[2] *Graduate Student Researcher, Dept. of Civil Engineering, Chiao Tung University, Hsinchu, Chinese Taiwan*
Email: cechou@ntu.edu.tw

ABSTRACT :

Cyclic tests on post-tensioned (PT) connections have demonstrated self-centering capabilities with gap opening, closing at the beam-to-column interface. When the gap opens at the beam-to-column interface in a real frame with more than one column, this gap opening is constrained by the columns. The columns provide flexural restraint to the beams, leading to the compression force different from the strand force in the beams. This study presents a methodology to evaluate the bending stiffness of the columns and the compression force in the beams by deforming a building-height column in accordance with gap opening responses at all connection levels. The predicted compression force in the beams is validated by a detailed 3-story PT frame analytical model and cyclic tests of a full-scale, two-bay by first-story PT frame. The proposed model shows that the beam compression force is increased at the 1st story but decreased at the 2nd and 3rd stories due to deformation compatibility of the whole column. The PT frame tests demonstrate that the proposed model reasonably predicts the beam compression force and strand force, and that the beam compression force at a 3% drift is 2% and 60% larger than the strand force with respective to a little restraint and pin-supported column boundary condition.

KEYWORDS: Post-tensioned Frame, Steel Beam, Column Restraint, Cyclic Frame Test

1. INTRODUCTION

A post-tensioned (PT) self-centering moment frame that uses post-tensioning steel to compress the steel beams against the columns has recently been developed as an alternative to a steel special moment-resisting frame (SMRF). Many researchers (Ricles et al. 2001, 2002, Christopoulos et al. 2002, Garlock 2002, Garlock et al. 2005, Chou et al. 2006, Tsai et al. 2008) have experimentally validated the self-centering behaviors of the PT connections with either energy yielding or friction damped devices. The issues of column and slab restraint raised by Christopoulos et al. (2002) and Garlock (2002) have been challenging subjects in this system. Chou et al. (2008a) experimentally showed that the proposed PT connection with a continuous composite slab self-centers with low residual deformation as long as negative connection moments provided by slab reinforcements are considered in design. Chou et al. (2008b) also demonstrated similar cyclic responses between a bare PT connection and a composite PT connection with a discontinuous composite slab, which opens freely along with the gap opening at the beam-to-column interface.

As the gap widens at the beam-to-column interface, leading to an expansion in the PT frame and bending in the columns, the compression force in the beams is affected by this restraint. Christopoulos et al. (2002) proposed a pin-pin supported column boundary condition for the upper stories and a pin-fixed supported column boundary condition for the first story to estimate the bending stiffnesses of the columns. The boundary condition does not include effects of the column above and below the story that is being considered, and deformation compatibility of the whole column is not considered, leading to an overestimation of the column bending stiffness. Instead, this study presents a methodology to evaluate the bending stiffness of the columns and compression force in the beams by deforming a whole column in accordance with gap opening responses at all connection levels. The predicted compression forces in the beams are close to those obtained by a detailed 3-story PT frame computer model and cyclic tests of a full-scale, two-bay by first-story PT frame.

2. DESIGN OF A 3-STORY POST-TENSIONED SELF-CENTERING BUILDING

Figs.1 (a) and (b) show the plan and elevation of the prototype building, which was assumed to be located on stiff soil in Los Angeles, California. The three two-bay PT frames provided lateral load resistance in the east-west direction; each PT frame was composed of three PT reinforced concrete columns and three PT steel beams. A reduced flange plate (RFP) proposed by Chou et al. (2006, 2008a) was incorporated at each beam-to-column connection to increase energy dissipation (Fig. 2(a)). The RFP moment connections (Chou and Wu 2007) were also demonstrated to eliminate steel beam buckling as observed in traditional welded moment connections subject to cyclic loads. No energy dissipation device was used at the PT column base (Fig. 2(b)).

The design dead loads were 5.28 kPa (110 psf) and 4.32 kPa (90 psf) for the floors and the roof while the live loads for the floors and the roof were 2.39 kPa (50 psf). Effective seismic weights for the floors and the roof were 2320 kN and 1896 kN, respectively, resulting in an effective seismic weight of the building of 6536 kN. The structural period, T, and the seismic response coefficient, C_s, calculated by the codified method (IBC 2000) were 0.6 sec and 0.125, respectively, so the seismic design base shear, V_{des}, for one PT frame was 272 kN. The beam and column sizes, RFP thickness (t_R) and narrowest dimension (b_R), strand and PT bar area (A_{ST}), and initial PT force (T_{in}) are given in Table 1. High strength Dywidag (DSI) bar was specified to the column PT bar, and ASTM A 706M steel was specified for the column transverse and longitudinal reinforcements. The specified 28-day concrete strength, f'_{cn}, was 28 MPa. A572 Grade 345 (50) steel was used for the steel beams, and ASTM A416 Grade 270 strands with each diameter of 15 mm were passed along the beam webs and anchored outside the exterior PT columns. Moment demands at the beam-to-column interface and the column base due to the seismic load (M_E), dead load (M_D), and live load (M_L) are also given in Table 1. The decompression moment of PT connections, M_d, listed in Table 1 is composed of the moments provided by the strands and the RFPs. The decompression moment is larger than the moment due to dead load and live load, but is slightly less than the combined moment demand, M_{dem}. The connection moment at the onset of RFP yielding, M_y, is larger than $\alpha_y M_{dem}$, where $\alpha_y \geq 1.0$ (Table 1), indicating that the PT frame remains elastic under the code-based seismic load. Following the connection design procedure proposed by Chou et al. (2008a), the connection moment at a roof drift of 4%, $M_{4\%}$, reached about $0.9M_{np}$, in which $M_R \approx 0.3M_{np}$ was provided by the RFPs and $M_{ST} \approx 0.6M_{np}$ was provided by the strands. A notation M_{np} represents the nominal plastic moment capacity of the beam.

Table 1 3-story PT frame dimension and moment

Story	Size (mm)	A_{ST} (mm^2)	T_{in} (kN)	t_R (mm)	b_R (mm)	$\frac{M_E}{M_{np}}$	$\frac{M_D}{M_{np}}$	$\frac{M_L}{M_{np}}$	$\frac{M_{dem}}{M_{np}}$	$\frac{M_d}{M_{np}}$	$\frac{M_y}{M_{np}}$	$\frac{M_{4\%}}{M_{np}}$
3rd	H320×160×7.5×13	1184	500	4	120	0.22	0.15	0.09	0.48	0.37	0.48	0.94
2nd	H500×200×10×16	1184	900	8	120	0.29	0.05	0.03	0.37	0.35	0.46	0.86
1st	H500×200×10×16	1579	900	8	120	0.34	0.05	0.03	0.42	0.35	0.46	0.91
Column	RC 650×650	4072	1100	-	-	0.24	-	-	0.24	0.2	-	-

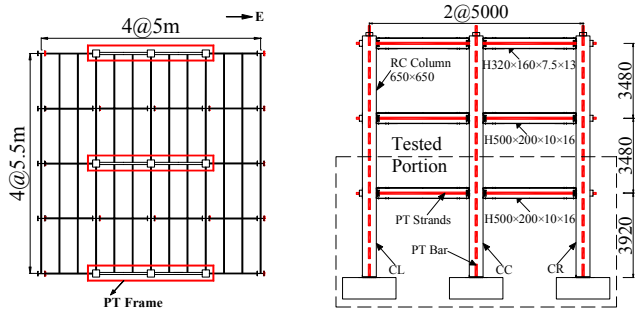

(a) Plan (b) Elevation (unit: mm)

Figure 1 Prototype building

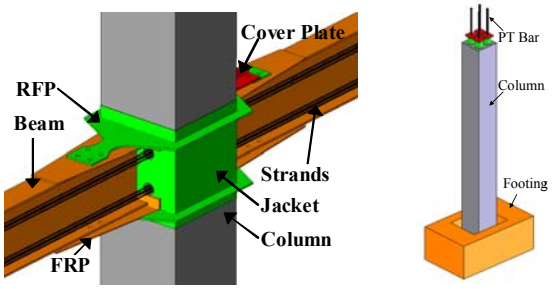

(a) PT connection (b) PT column

Figure 2 PT connection and column

3. MODELING OF A 3-STORY POST-TENSIONED SELF-CENTERING FRAME

Christopoulos et al. (2002) used a number of axial springs at the beam-to-column connection to capture the self-centering behavior of the frame. This axial spring (AS) modeling can capture the effects of constrained beams. Figs. 3(a) and (b) show the monotonic and cyclic force-deformation relationships of the 3-story PT frame based on this AS model. The normalized base shear was obtained by dividing the base shear by the value of V_{des} = 272 kN. The PT frame decompressed after the codified base shear V_{des}. The PT column base first opened (step A), followed by a consecutive gap opening of the beam-to-column interface at the 3rd, 1st, and 2nd stories, respectively. The yield strength of the PT frame was 490 kN (=1.8 V_{des}) at a roof drift about 0.5%. At a roof drift of 2% (DBE level for the SMRF), the maximum base shear reached 3V_{des}. Fig. 3(c) shows the expansion of the exterior columns CL and CR (Fig. 1(b)), which were computed by subtracting the exterior column lateral deformation by the central column lateral deformation. This expansion is caused by the gap opening response at the connection level, and is more pronounced for the first story than other stories due to fixity at the base. As can be seen from the analytical results, the strand force at the 1st story is 10-13% smaller than the beam compression force (Fig. 4(a)). However, the strand forces at the 2nd and 3rd stories are 2-4% and 7-8% larger than the beam compression force (Figs. 4(b) and (c)).

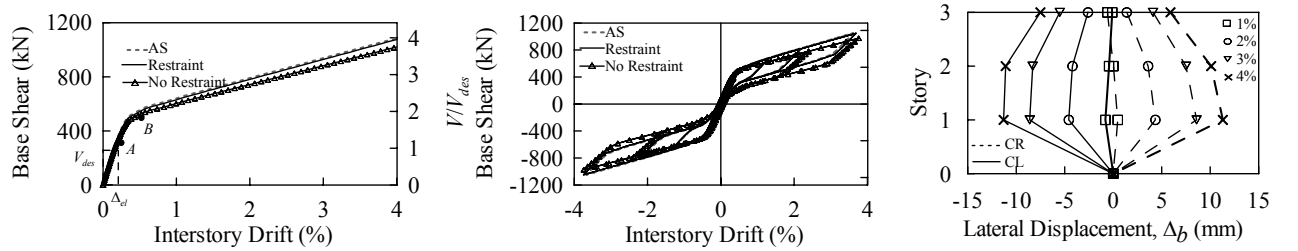

(a) Monotonic pushover analysis (b) Cyclic analysis (c) Frame expansion

Figure 3 PT frame response

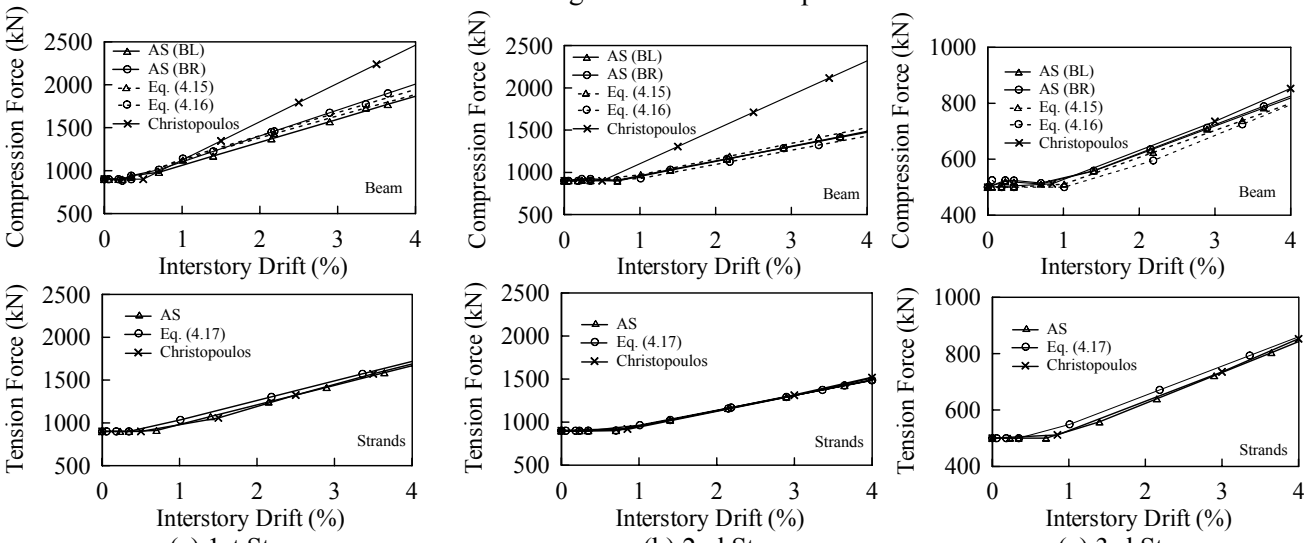

(a) 1st Story (b) 2nd Story (c) 3rd Story

Figure 4 Beam compression force and strand force

4. COMPRESSION FORCE PREDICTION IN THE PT BEAM

4.1. Rotational Spring Model

Instead of using axial springs at the PT connection, Chou et al. (2005) also proposed a rotational spring scheme to capture the self-centering response of the PT connection. As can be seen in Fig. 5(a), the intersection of the beam and column centerlines has three nodes *j*, *m*, and *n*. Two zero-length spring elements, connecting the nodes *j* and *m*, were used to model the bilinear elastic behavior of the PT strands (SC spring) and the bilinear elastoplastic behavior of the RFPs (RFP spring), respectively. A combination of these two rotational springs

predicts well the experimental results of a PT connection (Fig. 5(b)). However, the PT force in the strands, the compression force in the beams, and the column restraining effects could not be discovered in the prior study. The rotational spring scheme could also be adopted to model the self-centering behavior of the PT column. Fig. 6(a) shows two nodes *j* and *k* at the PT column base. One zero-length rotational spring, connecting the nodes *j* and *k*, was used to model the bilinear elastic behavior of the PT column. Before decompression, the elastic rotational stiffness of the PT column, K_{c1}, is approximated using that of a fully restrained column. After reaching the decompression moment of the PT column, $M_{d,c}$, in Fig. 6(b) the rotational stiffness, K_{c2}, is

$$K_{c2} = \frac{1}{\frac{1}{K_{c1}} + \frac{1}{K_{cbar}}} \tag{4.1}$$

where the rotational stiffness, K_{cbar}, is provided by the PT bars in the column

$$K_{cbar} = \left[\frac{d_c}{2L_{bar}} E_{bar} A_{bar} \left(1 - \frac{A_{bar}}{A_{bar} + A_g} \right) \right] \frac{d_c}{2} \tag{4.2}$$

where d_c is the column depth, E_{bar} is the elastic modulus of the PT bar, A_{bar} is the PT bar area, L_{bar} is the PT bar length, and A_g is the column sectional area.

4.2 Bending Stiffness of a PT Column at Connection Levels

Fig. 7(a) shows the 3-story PT frame in a deformed position. As the gap opens at the beam-to-column interface (Δ_{b1}, Δ_{b2}, and Δ_{b3} at the 1st, 2nd, and 3rd stories, respectively), the strands in the beam elongate and result in axial shortening of the beams and bending of the exterior columns CL and CR. In order to develop bending stiffness of the exterior column above the 1st story, Christopoulos et al. (2002) proposed a simple estimate by assuming that the column is pin-pin supported at stories above and below the story that is being considered. For the 1st story, the column is PT to the base and pin-supported at the 2nd story, so the bending stiffness, K_c, is

$$K_c = \frac{36(h_1 + h_2)(E_c I_c)^2 + 12(h_1 + h_2)^2 E_c I_c K_{c2}}{12h_1^2 h_2^2 E_c I_c + h_1^3 h_2^2 K_{c2}\left(3 + \frac{h_2}{h_1 + h_2}\right)} \tag{4.3}$$

where h_1 is the 1st story height, h_2 is the 2nd story height, E_c is the elastic modulus of the concrete, and I_c is the moment inertia of the column. Considering that the compression force in the beams along the bays is symmetric with respect to the center column (CC), the compression force, F_b, in the beams is obtained by including the PT force and the column restraining effects. Compared with those obtained from the detailed PT frame model (AS) described in the previous section, this simple analytical model overestimates the beam compression forces by 49 and 55% at the 1st and 2nd stories at a 4% drift (Figs. 4(a) and (b)).

Instead of using an assumed column boundary condition, this study utilizes a deformed column to develop its bending stiffness at each story. The deformed column shape considers: (1) a gap-opening response at each story above the ground level, (2) beam bearing locations at the respective column heights, and (3) column base rigidity, K_{c2}, after the gap opens. Figs. 7(b) and (c) show deformed shapes (shape 3) for the two exterior columns CL and CR. A rotational spring with stiffness K_{c2} is positioned at the column base to simulate restraining of the base after the gap opens. At each story, the column CL has a specified lateral displacement, Δ_b ($=\theta_g(d_b - t_f)$), at a location of the beam top flange inner side, and the column CR has the same specified lateral displacement, Δ_b, at a location of the beam bottom flange inner side, where d_b is the beam depth and t_f is the flange thickness. Assuming the same gap opening angles (e.g. θ_g=0.01 rad.) at the column base and each connection, numbers, 4.84 and 3.07 mm marked in the figure, are the lateral displacements Δ_b specified at each story. The bending stiffnesses of the columns CL and CR at each story are K_{cl} and K_{cr}, respectively, which are computed by dividing the corresponding reaction force, F_{cl} and F_{cr}, by the lateral displacement Δ_b. The column bending stiffnesses, K_{cl} and K_{cr}, at each story are different and negative at the 2nd and 3rd stories due to a specified column deformation, leading to a reduced compression force in the beams.

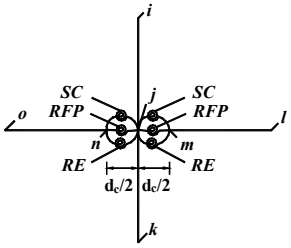

(a) PT connection model

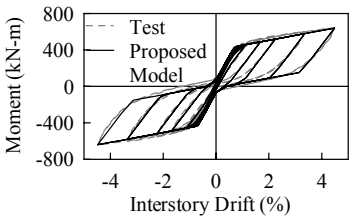

(b) Moment-drift relationship

Figure 5 PT connection modeling

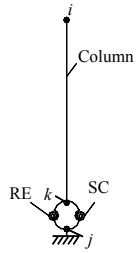

(a) Column model

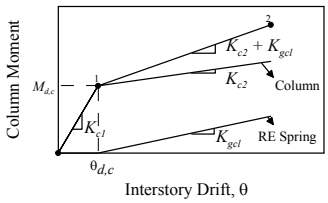

(b) Column behavior

Figure 6 PT column modeling

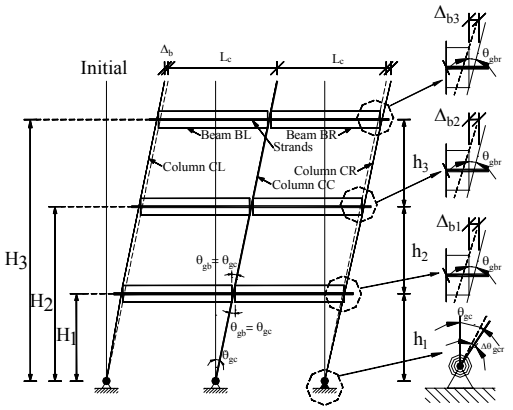

(a) PT frame deformation

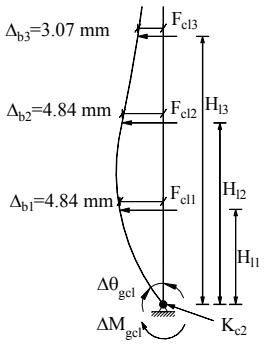

(b) Column CL

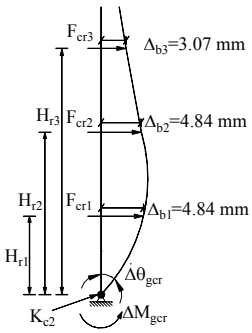

(c) Column CR

Figure 7 3-story PT frame and exterior column deformation

4.3. PT Beam Compression Load

The exterior columns CL and CR bear against opposite sides of the beams BL and BR at the same drift, resulting in different bending stiffnesses (or restraints) of the exterior columns to the PT beams. At any story, considering incremental equilibrium equations of horizontal force for the columns CL and CR:

$$\Delta F_{bl} = \Delta F_{cl} + \Delta T_{ST} \tag{4.4}$$

$$\Delta F_{br} = \Delta F_{cr} + \Delta T_{ST} \tag{4.5}$$

where ΔF_{bl} and ΔF_{br} are the incremental compression forces in the beams BL and BR, respectively; ΔF_{cl} and ΔF_{cr} are the incremental restraining forces of the columns CL and CR, respectively, and ΔT_{ST} is the incremental strand force. The incremental shortening of the left beam BL due to the increased compression force is:

$$\delta_{bl} = \delta_{ST} + \delta_{cl} \tag{4.6}$$

where δ_{cl} is the component of the beam BL shortening due to the column CL incremental restraining force (ΔF_{cl}), and δ_{ST} is the component of the beam shortening due to the incremental strand force ΔT_{ST}. The column CL incremental restraining force is

$$\Delta F_{cl} = K_b \delta_{cl} = K_{cl}\left(\Delta_b - \delta_{ST} - \delta_{cl}\right) \tag{4.7}$$

Where K_b is the axial stiffness of the beam. Rearranging Eq. (4.7), the component of the beam BL shortening due to the column CL incremental restraining is

$$\delta_{cl} = \frac{K_{cl}}{K_{cl} + K_b}\left(\Delta_b - \delta_{ST}\right) \tag{4.8}$$

The component of the beam BR shortening due to the column CR incremental restraining is also expressed as

$$\delta_{cr} = \frac{K_{cr}}{K_{cr} + K_b}\left(\Delta_b - \delta_{ST}\right) \tag{4.9}$$

The ratio of the two beam shortenings due to column incremental restraining effects is

$$\varsigma = \frac{\delta_{cr}}{\delta_{cl}} = \frac{K_{cr}\left(K_{cl}+K_b\right)}{K_{cl}\left(K_{cr}+K_b\right)} \tag{4.10}$$

Since the column bending stiffnesses, K_{cl} and K_{cr}, are different, the ratio,ζ , ranges from 0.7-1.9. The strand force increment, ΔT_{ST}, is

$$\Delta T_{ST} = K_b \delta_{ST} = K_{ST}\left[2\Delta_b - 2\delta_{ST} - (1+\varsigma)\delta_{cl}\right] \tag{4.11}$$

where K_{ST} is the axial stiffness of the strands. Rearranging Eq. (4.11), the component of the beam shortening due to the incremental strand force is

$$\delta_{ST} = \frac{K_{ST}}{2K_{ST}+K_b}\left[2\Delta_b - (1+\varsigma)\delta_{cl}\right] \tag{4.12}$$

Substituting Eq. (4.12) into Eqs. (4.8) and (4.9), the components of the beam BL and BR shortenings due to the column incremental restraining forces are:

$$\delta_{cl} = \frac{K_{cl}K_b}{\left(K_{cl}+K_b\right)\left(2K_{ST}+K_b\right)+(1+\varsigma)K_{ST}K_{cl}}\Delta_b \tag{4.13}$$

$$\delta_{cr} = \frac{\varsigma K_{cl}K_b}{\left(K_{cl}+K_b\right)\left(2K_{ST}+K_b\right)+(1+\varsigma)K_{ST}K_{cl}}\Delta_b \tag{4.14}$$

For a specific gap opening Δ_b, the beam BL and BR forces, F_{bl} and F_{br}, and the strand force, T_{ST}, are:

$$F_{bl} = T_{in} + \Delta F_{bl} = T_{in} + K_b\left(\delta_{ST} + \delta_{cl}\right) \tag{4.15}$$

$$F_{br} = T_{in} + \Delta F_{br} = T_{in} + K_b\left(\delta_{ST} + \delta_{cr}\right) \tag{4.16}$$

$$T_{ST} = T_{in} + K_b\delta_{ST} \tag{4.17}$$

Fig. 4 shows predictions based on Eqs. (4.15)-(4.17), which are close to those obtained from the detailed frame model using axial springs (ASs). The predicted beam compression force is larger than the strand force at the first story and smaller than the strand force at the 2nd and 3rd stories due to negative column bending stiffnesses. The reduction of the beam compression force from the applied strand force at the 2nd and 3rd stories could not be obtained from the simple estimate proposed by Christopoulos et al. (2002) because the column deformation shape was not considered in developing bending stiffness. It was also found that although the compression toes in beams BL and BR differ by a beam depth, the compression force variation, $K_b\delta_{cl}$ and $K_b\delta_{cr}$, show minor different compared to the strand force, T_{ST}, indicating that the beam-to-column centerline intersection can be used as a compression location for simplicity. In this case, the column bending stiffness at each story, K_{cc}, can be computed by deforming the column at the specified lateral displacement, Δ_b, and associated reaction forces. The resulting beam axial force is 12% larger than the strand force at the first story and 3-4% lower than the strand force at the 2nd and 3rd stories.

5. PT FRAME TEST

To evaluate the effects of column restraining on the frame expansion, a full-scale, two-bay by first-story PT frame (marked in Fig. 1(b)) was cyclically tested. A total of twelve ASTM A416 Grade 270 strands with each diameter of 15 mm were passed along the beam web, through three PT columns, and anchored outside the exterior columns. The initial PT forces in the columns and beams were about 1100 kN and 916 kN, respectively; a total of four cyclic tests were conducted on this frame (Fig. 8). Each column was extended to the mid-height of the second story, at which two 1000 kN actuators (labeled as Act 1 and Act 2) were positioned between the reaction wall and the frame and one 1000 kN actuator (labeled as Act3 and Act 4) was positioned between each beam span. Quasi-static cyclic loading with increasing displacement amplitude in accordance to AISC (2005) for connection tests was adopted. The displacement of the column CC was controlled as a target displacement; the interstory drift was defined as the horizontal displacement at the loading point relative to the column height of 5.66 m. Two loading schemes were adopted in the test program. For the first loading scheme, the forces in Act 3 and Act 4 were slaved, respectively, to three-quarter and one-quarter the summation of the forces in Act 1 and Act 2. Therefore, the shear applied to the columns CL and CR would be half of that applied to the column CC at the loading point to simulate little restraint on the top of the columns. This loading scheme was carried out for the first three tests, in which RFPs for energy dissipation were only included in the

connections for the first two tests. For the second loading scheme, no relative lateral deformation was allowed between the columns to simulate a full restraint on the top of the columns. No energy dissipation devices were provided at the column base.

In the first cyclic test, two out of eight RFPs fractured when the frame moved towards an interstory drift of 4% (Fig. 9). The frame was retested using the same loading protocol, and no more RFPs fractured in the 2nd tests. Fig. 10(a) shows the base shear versus column CC deformation for the first two tests; it appears that the PT frame under the 1st test dissipated larger energy than the 2nd test. Six RFPs were removed from the frame after the 2nd test in order to evaluate the frame response without energy dissipating devices. The bilinear elastic behavior of the PT frame was observed by comparing the hysteretic loops between the 1st and 3rd tests (Fig. 10(b)). For the 4th test, the PT frame was loaded with no relative column deformation at the level of actuators, so the post-yielding stiffness of the frame was 20% higher in the 4th test than in the 3rd test. Considering horizontal and vertical force equilibriums in the three columns and taking moment equilibriums about column compression toes, the compression force in the beams BL and BR (Fig. 11) were obtained from the tests. Fig. 11 shows strand forces and compression forces in the beam for the 3rd and 4th tests. The beam compression force is similar to the beam strand force in the 3rd test (Figs. 11(a) and (b)), in which the column top can expand during the test. Two tests resulted in similar strand force in the beams, but the beam compression force is 60% larger than the beam strand force in the 4th test (Fig. 11(c)) because the distance between each column top does not vary during the test. Following the same procedure described earlier, the exterior column bending stiffnesses, K_{cc}, are 862 and 73366 kN/m for the 3rd and 4th tests, respectively. The resulting beam compression forces based on Eqs. (4.15) and (4.16) with K_{cc} for both column bending stiffnesses agree well the test results (Fig. 11).

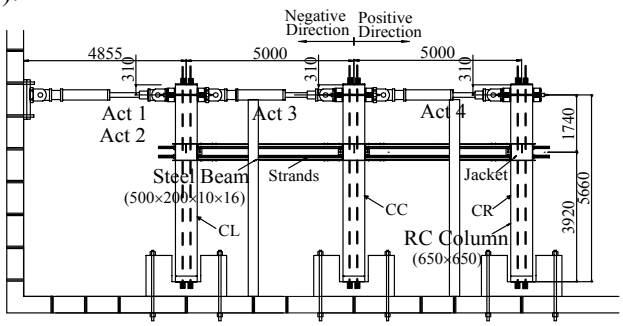

Figure 8 Test setup (unit: mm)

Figure 9 PT frame deformation (4% drift)

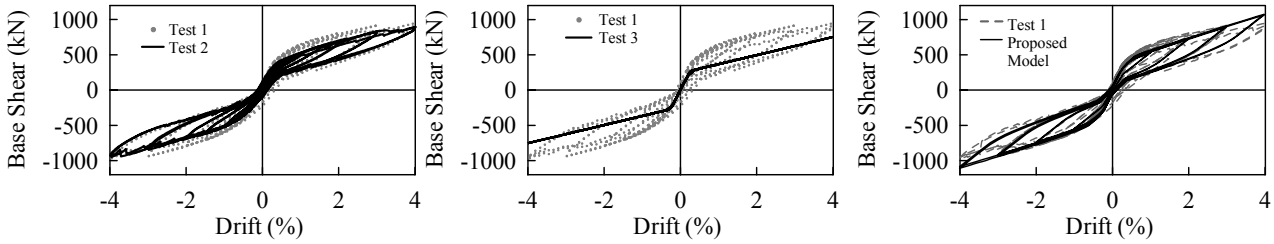

(a) Test 1 versus test 2 (b) Test 1 versus test 3 (c) Test 1 versus prediction

Figure 10 Hysteretic responses of PT frame tests

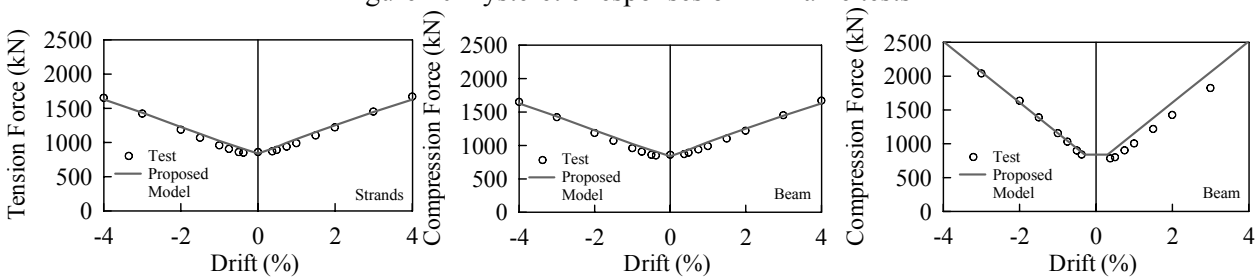

(a) Strand force (3rd test) (b) Beam compression force (3rd test) (c) Beam compression force (4th test)

Figure 11 Beam strand and compression force in 3rd and 4th PT frame tests

6. CONCLUSIONS

This paper presents a methodology to take into account the PT frame expansion. The procedure is aimed at (1) deforming a building-height column in accordance with gap opening responses at all connection levels, and (2) computing the column bending stiffness at each story by the reaction force divided by the respective lateral displacement. Because this deformed column shape includes effects of the column above and below the story that is being considered, the column bending stiffness at each story is more realistic and smaller than those developed based on a pin-pin supported column boundary condition. The following conclusions are made:

(1) For the 3-story PT frame, the beam compression force is larger than the beam strand force at the 1st story, but smaller than the beam strand force at the 2nd and 3rd stories due to column deformation compatibility. The variation of the beam compression force can be reasonably predicted based on the proposed model in this study. However, the simple estimate based on an assumed column boundary condition always predicts the increased compression force in the beam and the overestimation of the beam compression force is about 50% at the 1st and 2nd stories.

(2) A full-scale, two-bay by first-story PT frame was cyclically tested. Two loading schemes were conducted on the test frame to evaluate the column restraints. The first loading scheme produced the shear in the exterior columns half of that in the center column to simulate little restraint from the column to the PT beam. The second loading scheme produced no relative lateral deformation between columns to simulate a pin-supported column boundary at the column top. The two loading schemes resulted in similar beam strand force but significant different compression force in the beam; the beam compression force is 60% larger than the beam strand force in the second loading scheme.

ACKNOWLEDGEMENTS

The test program was supported by the NCREE with Prof. K. C. Tsai as the program director. The writers are grateful to Prof. H.L. Hsu of NCU and Dr. K.C. Lin of NCREE for corporation on design of the tested frame.

REFERENCES

Christopoulos, C., Filiatrault, A., and Uang, C-M. (2002). Self-centering post-tensioned energy dissipating (PTED) steel frames for seismic regions. *Report No. SSRP-2002/06*, Dept.of Structural Eng., University of California, San Diego, CA.

Christopoulos, C., Filiatrault, A., Uang, C-M, and Folz, B. (2002). Posttensioned energy dissipating connections for moment-resisting steel frames. *Journal of Structural Engineering*, 128(9), 1111-1120.

Chou, C-C, Tsai, K-C, Chen, J-H, Chen, Y-C, and Jhuang, S-C. (2005). Cyclic behavior of post-tensioned steel connections with reduced flange plate and slab. *1st International Conference on Advances in Experimental Structural Engineering*, Nagoya, Japan.

Chou, C-C, Chen, J-H, Chen, Y-C, and Tsai, K-C. (2006). Evaluating performance of post-tensioned steel connections with strands and reduced flange plates. *Earthquake Engineering and Structural Dynamics*, 35(9), 1167-1185.

Chou, C-C and Wu, C-C. (2007). Performance evaluation of steel reduced flange plate moment connections. *Earthquake Engineering and Structural Dynamics*, 36, 2083-2097.

Chou, C-C, Wang, Y-C, Chen, J-H. (2008a). Seismic design and behavior of post-tensioned steel connections including effects of a composite slab. *Engineering Structures*. (available online May 2008).

Chou, C-C, Tsai, K-C, and Yang, W-C. (2008b). Self-centering steel connections with steel bars and a discontinuous composite slab. *Earthquake Engineering and Structural Dynamics*. (accepted for publication).

Garlock, M.M. (2002). Full-scale testing, seismic analysis, and design of post-tensioned seismic resistant connections for steel frames. *Ph.D. dissertation*, Civil and Environmental Eng. Dept., Lehigh Univ., PA.

Garlock, M.M, Ricles, M.J, and Sause, R. (2005). Experimental studies of full-scale posttensioned steel connections. *Journal of Structural Engineering*, 131(3), 438-448.

Ricles, J.M., Sause, R., Garlock, M.M. and Zhao, C. (2001). Posttensioned seismic-resistant connections for steel frames. *Journal of Structural Engineering*, 127(2), 113–121.

Ricles, J.M, Sause, R., Peng, S.W., and Lu, L.W. (2002). Experimental evaluation of earthquake resistant posttensioned steel connections. *Journal of Structural Engineering*, 128(7), 850-859.

Tsai, K-C, Chou, C-C, Lin, C-L, Chen, P-C, Jhang, S-J. (2008). Seismic self-centering steel beam-to-column moment connections using bolted friction devices. *Earthquake Engineering and Structural Dynamics,* 37, 627-645.